J. Fluid Mech. (2019), *vol.* 878, *pp.* 502–521. © Cambridge University Press 2019
doi:10.1017/jfm.2019.634

Stokes waves with constant vorticity: folds, gaps and fluid bubbles

Sergey A. Dyachenko[1,2,†] **and Vera Mikyoung Hur**[1]

[1]Department of Mathematics, University of Illinois at Urbana-Champaign, Urbana, IL 61801, USA

[2]Department of Applied Mathematics, University of Washington, Seattle, WA 98195, USA

(Received 1 March 2019; revised 12 July 2019; accepted 22 July 2019;
first published online 17 September 2019)

The Stokes wave problem in a constant vorticity flow is formulated, by virtue of conformal mapping techniques, as a nonlinear pseudodifferential equation, involving the periodic Hilbert transform, which becomes the Babenko equation in the irrotational flow setting. The associated linearized operator is self-adjoint, whereby the modified Babenko equation is efficiently solved by the Newton-conjugate gradient method. For strong positive vorticity, a 'fold' appears in the wave speed versus amplitude plane, and a 'gap' as the vorticity strength increases, bounded by two touching waves, whose profile contacts with itself at the trough line, enclosing a bubble of air. More folds and gaps follow for stronger vorticity. Touching waves at the beginnings of the lowest gaps tend to the limiting Crapper wave as the vorticity strength increases indefinitely or, equivalently, gravitational acceleration vanishes, while the profile encloses a circular bubble of fluid in rigid body rotation at the ends of the gaps. Touching waves at the beginnings of the second gaps tend to the circular vortex wave on top of the limiting Crapper wave in the infinite vorticity limit, or the zero gravity limit, and the circular vortex wave on top of itself at the ends of the gaps. Touching waves for higher gaps accommodate more circular bubbles of fluid.

Key words: surface gravity waves

1. Introduction

Stokes (1847, 1880) made formal but far-reaching considerations about periodic waves at the surface of an incompressible inviscid fluid in two dimensions, subject to the force of gravity, propagating a long distance at a practically constant velocity without change of form. For instance, he observed that the crests become sharper and the troughs flatter as the amplitude increases, and that the wave of greatest height, or the extreme wave, is distinguished by a 120° peaking at the crest. It would be impossible to give here a complete account of Stokes waves. We merely pause to remark that in the irrotational flow setting, notable recent advances were based on a formulation of the problem as a nonlinear pseudodifferential equation, due to Babenko (1987) and others. For instance, Dyachenko, Lushnikov & Korotkevich (2016), Lushnikov (2016), Lushnikov, Dyachenko & Silantyev (2017) revealed the complex singularities of almost extreme waves in meticulous detail.

† Email address for correspondence: sdyachen@math.uiuc.edu

https://doi.org/10.1017/jfm.2019.634 Published online by Cambridge University Press

The irrotational flow assumption is well justified in some circumstances. But rotational effects are significant in many others. Water waves are commonly generated by wind, and in any region where wind blows, there is a surface drift of water, which may considerably influence the maximum wave height and other quantities. Moreover, currents produce shear at the bed of the sea or a river, which may drastically alter waves in shallow water (see Peregrine 1976, § IV, for instance).

Constant vorticity is of particular interest because of its analytical tractability. Moreover, when waves are short compared with the characteristic length scale of vorticity, it is the value of the vorticity at the fluid surface that is more important than its specific distribution (see Teles da Silva & Peregrine 1988, for instance). In a continental selve and shallow sea, a wind generated current is well described by non-zero mean vorticity (see Ewing 1990, for instance). For tidal currents, positive and negative constant vorticity are appropriate for the ebb and flood (see Swan, Cummins & James 2001, for instance). Here we distinguish negative vorticity for waves propagating downstream, and positive vorticity for upstream (see Teles da Silva & Peregrine 1988, for instance).

Dyachenko & Hur (2019) modified the Babenko equation and supplemented it with a scalar constraint, to allow constant vorticity and finite depth, and numerically solved using the Newton-generalized minimum residual (GMRES) method. In § 2, we exploit a change of variables to eliminate the Bernoulli constant from the equation and, hence, the scalar constraint. The associated linearized operator becomes self-adjoint. In § 3, we efficiently solve the modified Babenko equation using the Newton-conjugate gradient method. We achieve a high numerical precision for large amplitude waves for unprecedentedly large values of constant vorticity. Moreover, in § 2, we modify the equations in Zakharov, Dyachenko & Vasilyev (2002), for instance, for unsteady waves, to allow constant vorticity. These equations are potentially useful for studying stability, among others.

Simmen & Saffman (1985) discovered, and Dyachenko & Hur (2019) rediscovered, that for a large value of positive constant vorticity, a fold appears in the wave speed versus amplitude plane, and a gap of 'inadmissible' solutions as the value of the vorticity increases, bounded by two touching waves, whose profile contacts with itself at the trough line, enclosing a bubble of air. In § 4.1, we find more folds and gaps as the value of the vorticity increases further. See figure 5, for instance, for five folds and five gaps. We merely pause to remark that the numerical method of Simmen & Saffman (1985), Teles da Silva & Peregrine (1988) and others diverges in a gap, whence it is incapable of finding admissible solutions in higher folds.

Moreover, Dyachenko & Hur (2019) discovered that touching waves at the beginnings of the lowest gaps tend to the limiting Crapper wave (see Crapper 1957, for instance) as the value of positive constant vorticity increases indefinitely or, equivalently, gravitational acceleration vanishes, while the profile encloses a circular bubble of fluid in rigid body rotation at the ends of the gaps. In § 4.2, we find the circular vortex wave on top of the limiting Crapper wave at the beginning of the second gap in the infinite vorticity limit, or the zero gravity limit, and the circular vortex wave on top of itself at the end of the gap. We find more circular bubbles of fluid at the boundaries of higher gaps in the infinite vorticity limit. See figure 9, for instance, for a profile nearly enclosing five circular bubbles of fluid.

The constant vorticity assumption is simplified, whence some details of the waves reported herein may be of academic interest. But their prominent features are significant for potential applications to waves in a stream and the effects of wind generated currents. For instance, steep and rounded waves resemble those at beaches

https://doi.org/10.1017/jfm.2019.634 Published online by Cambridge University Press

in the backwash from surf (see Teles da Silva & Peregrine 1988, for instance). We draw particular attention to a striking and surprising link between rotational and capillary effects. Moreover, the instability of a large amplitude wave and its possible stabilization may be relevant to some physical processes.

2. Formulation

We consider a two-dimensional, infinitely deep and constant vorticity flow of an incompressible inviscid fluid, subject to the force of gravity, and the wave motion at the interface between the fluid and air. We assume for simplicity a unit fluid density. Suppose that in Cartesian coordinates, the x axis points in the direction of wave propagation, and the y axis vertically upward. Suppose that the fluid occupies a region $\Omega(t)$ in the (x, y) plane at time t, bounded above by a free surface $\Gamma(t)$.

Let $\boldsymbol{u} = \boldsymbol{u}(x, y, t)$ denote the velocity of the fluid at the point (x, y) and time t, and $P = P(x, y, t)$ the pressure. They satisfy the Euler equations for an incompressible fluid

$$\boldsymbol{u}_t + (\boldsymbol{u} \cdot \nabla)\boldsymbol{u} = -\nabla P + (0, -g) \quad \text{and} \quad \nabla \cdot \boldsymbol{u} = 0 \quad \text{in } \Omega(t), \tag{2.1a,b}$$

where g is the constant of gravitational acceleration. Throughout, we assume that the vorticity

$$\omega = \nabla \times \boldsymbol{u} \tag{2.2}$$

is constant. The kinematic and dynamic boundary conditions

$$\partial_t + \boldsymbol{u} \cdot \nabla \quad \text{is tangent to } \bigcup_t \Gamma(t) \quad \text{and} \quad P = P_{atm} \text{ at } \Gamma(t) \tag{2.3a,b}$$

state that the velocity of the fluid surface is given by the normal component of the velocity of the fluid and that the pressure at the fluid surface equals the constant atmospheric pressure P_{atm}. We neglect the effects of surface tension. We assume that Ω, and $\boldsymbol{u}$, P are periodic in the x variable. We may take without loss of generality that the period is 2π.

Suppose that

$$\boldsymbol{u}(x, y, t) = (-\omega y, 0) + \nabla\phi(x, y, t) \tag{2.4}$$

for $(x, y) \in \Omega(t)$, whence

$$\Delta\phi = 0 \quad \text{in } \Omega(t) \tag{2.5}$$

by the latter equation of (2.1). We merely pause to remark that for any $\omega \in \mathbb{R}$,

$$\Omega(t) = \{(x, y) \in \mathbb{R}^2 : y < 0\}, \quad \boldsymbol{u}(x, y, t) = (-\omega y, 0) \quad \text{and} \quad P(x, y, t) = P_{atm} - gy \tag{2.6a–c}$$

solve (2.1) and (2.3) at all times. Here we assume that some external effects produce constant vorticity and we restrict our attention to waves propagating in the rotational flow. For non-constant vorticity, (2.4) and (2.5) are inapplicable.

https://doi.org/10.1017/jfm.2019.634 Published online by Cambridge University Press

Substituting (2.4) into the former equation of (2.1) and using the latter equation of (2.3), we make an explicit calculation to arrive at

$$\phi_t + \tfrac{1}{2}|\nabla\phi|^2 - \omega y\phi_x + \omega\psi + gy = b(t) \quad \text{at } \Gamma(t) \tag{2.7}$$

for some function b, where ψ is a harmonic conjugate of ϕ.

The boundary condition in the infinite depth is that

$$\phi, \psi \to 0 \quad \text{as } y \to -\infty \quad \text{uniformly for } x \in \mathbb{R}. \tag{2.8}$$

In the finite depth, we replace (2.8) by

$$\phi_y = 0 \quad \text{at } y = -h \quad \text{for some } h > 0 \tag{2.9}$$

and proceed in like manner (see Dyachenko & Hur 2019, for instance, for details). The effects of finite depth will change the amplitude of a Stokes wave and other quantities (see Dyachenko & Hur 2019, for details).

2.1. *Reformulation in conformal coordinates*

We proceed as in Dyachenko & Hur (2019), and reformulate (2.1), (2.3) and (2.8) more conveniently in conformal coordinates. In the irrotational flow setting, we refer the interested reader to Dyachenko *et al.* (1996), Zakharov *et al.* (2002), among others. In what follows, we identify $\mathbb{R}^2$ with $\mathbb{C}$ whenever it is convenient to do so.

Suppose that

$$z(u + \mathrm{i}v, t) = (x + \mathrm{i}y)(u + \mathrm{i}v, t) \tag{2.10}$$

conformally maps $\mathbb{C}^- := \{u + \mathrm{i}v \in \mathbb{C} : v < 0\}$ of 2π period in the u variable, to $\Omega(t)$ of 2π period in x, at time t, and that $z(u + \mathrm{i}v) \to u + \mathrm{i}v$ as $v \to -\infty$. Suppose that (2.10) extends to map $\{u + \mathrm{i}0 : u \in \mathbb{R}\}$ to $\Gamma(t)$.

Since $z - (u + \mathrm{i}v)$ is holomorphic in $\mathbb{C}^-$ and it is 2π periodic in the u variable by hypothesis,

$$z(u, t) = u + (\mathcal{H} + \mathrm{i})y(u, t) \quad \text{for } u \in \mathbb{R}, \tag{2.11}$$

(see Zygmund 1959, for instance). Here and elsewhere, $\mathcal{H}$ denotes the periodic Hilbert transform, defined by

$$\mathcal{H}e^{iku} = -\mathrm{i}\,\mathrm{sgn}(k)\mathrm{e}^{\mathrm{i}ku} \quad \text{for } k \in \mathbb{Z} \tag{2.12}$$

and extended by linearity and continuity. Therefore,

$$\Gamma(t) = \{(u + \mathcal{H}y(u, t), y(u, t)) : u \in \mathbb{R}\}. \tag{2.13}$$

Moreover, let

$$F(u + \mathrm{i}v, t) = (\phi + \mathrm{i}\psi)(z(u + \mathrm{i}v, t), t) \quad \text{for } u + \mathrm{i}v \in \mathbb{C}^-. \tag{2.14}$$

Since F is holomorphic in $\mathbb{C}^-$ by (2.5) and it is 2π periodic in the u variable by hypothesis,

$$F(u, t) = (1 - \mathrm{i}\mathcal{H})\phi(u, t) \quad \text{for } u \in \mathbb{R}. \tag{2.15}$$

https://doi.org/10.1017/jfm.2019.634 Published online by Cambridge University Press

Substituting (2.11) and (2.15) into the former equation of (2.3), we make an explicit calculation to arrive at

$$(1+\mathcal{H}y_u)y_t - y_u\mathcal{H}y_t - \mathcal{H}_d\phi_u - \omega y y_u = 0. \tag{2.16a}$$

Substituting (2.11) and (2.15) into (2.7), likewise, we make an explicit calculation to arrive at

$$\begin{aligned}&((1+\mathcal{H}y_u)^2+y_u^2)(\phi_t-\omega\mathcal{H}\phi+gy-b(t))\\&\quad-((1+\mathcal{H}y_u)\mathcal{H}y_t+y_uy_t)\phi_u+(y_u\mathcal{H}y_t-(1+\mathcal{H}y_u)y_t)\mathcal{H}\phi_u\\&\quad+\tfrac{1}{2}(\phi_u^2+(\mathcal{H}\phi_u)^2)-\omega y((1+\mathcal{H}y_u)\phi_u-y_u\mathcal{H}\phi_u)=0.\end{aligned} \tag{2.16b}$$

They form what Dyachenko & Hur (2019), for instance, derived. Conversely, a solution of (2.16) gives rise to a solution of (2.1), (2.3) and (2.8), provided that

$$u\mapsto(u+\mathcal{H}y(u,t),y(u,t)),\ u\in\mathbb{R},\ \text{ is injective} \tag{2.17}$$

and

$$((1+\mathcal{H}y_u)^2+y_u^2)(u,t)\neq 0\quad\text{for any } u\in\mathbb{R}. \tag{2.18}$$

See Dyachenko & Hur (2019), for instance, for details. An integration of (2.16*a*) over one period reveals that we may take without loss of generality that

$$\langle y(1+\mathcal{H}y_u)\rangle = 0 \tag{2.19}$$

at all times. Here and elsewhere, $\langle f\rangle$ denotes the average of a 2π periodic function f over one period.

Moreover, we solve (2.16) for y_t and ϕ_t and, hence, z_t and F_t in the complex form. The result becomes, after an explicit calculation,

$$\left.\begin{aligned}z_t&=\mathrm{i}\alpha z_u,\\F_t&=\mathrm{i}\alpha F_u-\beta+\frac{1}{2}\omega\mathcal{P}\left((z-z^*)\left(\frac{F_u}{z_u}+\frac{F_u^*}{z_u^*}\right)\right)+\mathrm{i}\omega F+\mathrm{i}g(z-u)+b(t),\end{aligned}\right\} \tag{2.20}$$

where

$$\alpha=\mathcal{P}\left(\frac{F_u-F_u^*+\frac{1}{2}\omega(z-z^*)(z_u-z_u^*)}{|z_u|^2}\right)\quad\text{and}\quad\beta=\mathcal{P}\left(\frac{|F_u|^2}{|z_u|^2}\right), \tag{2.21a,b}$$

and $\mathcal{P}=\frac{1}{2}(1-\mathrm{i}\mathcal{H})$. Here and elsewhere, the asterisk denotes complex conjugation. See Dosaev, Troitskaya & Shishina (2017), for instance, for details. The imaginary part of the former equation of (2.20) and the real part of the latter form what Dyachenko & Hur (2019), for instance, derived. In the irrotational flow setting, they become what Dyachenko *et al.* (1996), for instance, derived.

Furthermore, let

$$R=\frac{1}{z_u}\quad\text{and}\quad V=\mathrm{i}\frac{F_u}{z_u}. \tag{2.22a,b}$$

We solve (2.20) for R and V, to arrive at

$$\left.\begin{aligned}R_t&=\mathrm{i}(\alpha R_u-\alpha_u R),\\V_t&=\mathrm{i}(\alpha V_u-\beta_u R)+\tfrac{1}{2}\mathrm{i}\omega R((z-z^*)\mathcal{P}(V+V^*))_u+\mathrm{i}\omega V+g(R-1).\end{aligned}\right\} \tag{2.23}$$

See Dosaev *et al.* (2017), for instance, for details. In the irrotational flow setting, (2.23) becomes the so-called Dyachenko equations (see Zakharov *et al.* 2002, for instance), which are particularly convenient for numerical solution.

https://doi.org/10.1017/jfm.2019.634 Published online by Cambridge University Press

2.2. *The Stokes wave problem*

We turn our attention to travelling waves of (2.20), for which $z(u,t)-u$ and $F(u,t)$ are functions of $u-ct$ for some $c>0$, the speed of wave propagation, and $b(t)$ a constant. Under this assumption, we will go to a moving coordinate frame, changing $u-ct$ to u, whereby t completely disappears. The former equation of (2.20) becomes

$$\phi' = \mathcal{H}(\omega y y' + c y'). \tag{2.24}$$

Here and elsewhere, the prime denotes ordinary differentiation in the u variable. The latter equation of (2.20), after an explicit calculation, simplifies to

$$(c^2+2b-2gy)((1+\mathcal{H}y')^2+(y')^2)-(c+\omega y(1+\mathcal{H}y')-\omega\mathcal{H}(yy'))^2=0. \tag{2.25}$$

See Dyachenko & Hur (2019), for instance, for details.

2.3. *Reformulation as the modified Babenko equation*

We proceed as in Constantin, Strauss & Vărvărucă (2016), Dyachenko & Hur (2019), and reformulate (2.25) more conveniently as an equation of the Babenko kind. This makes use of the fact that $\mathcal{H}+\mathrm{i}$ determines the boundary value of a holomorphic and 2π periodic function in $\mathbb{C}^-$ up to the addition by a real constant (see Zygmund 1959, for instance).

We begin by rearranging (2.25) as

$$\begin{aligned}&(c^2+2b-2gy-\omega^2y^2)((1+\mathcal{H}y')^2+(y')^2)\\&\quad-2\omega y(c-\omega\mathcal{H}(yy'))(1+\mathcal{H}y')=(c-\omega\mathcal{H}(yy'))^2-\omega^2y^2(y')^2.\end{aligned} \tag{2.26}$$

Note that $(c-\omega(\mathcal{H}+\mathrm{i})(yy'))^2$ is the boundary value of a holomorphic and 2π periodic function in $\mathbb{C}^-$, and so is

$$(c^2+2b-2gy-\omega^2y^2)((1+\mathcal{H}y')^2+(y')^2)-2\omega y(c-\omega\mathcal{H}(yy'))(1+\mathcal{H}y'+\mathrm{i}y'). \tag{2.27}$$

Note that $1/(1+\mathcal{H}y'+\mathrm{i}y')$ is the boundary value of the holomorphic and 2π periodic function $1/z_u$ in $\mathbb{C}^-$, and so is $(c^2+2b-2gy-\omega^2y^2)(1+\mathcal{H}y'-\mathrm{i}y')-2\omega y(c-\omega\mathcal{H}(yy'))$. Therefore,

$$(c^2+2b-2gy-\omega^2y^2)(1+\mathcal{H}y')-2\omega y(c-\omega\mathcal{H}(yy'))=\mathcal{H}(-(c^2+2b-2gy-\omega^2y^2)y') \tag{2.28}$$

up to the addition by a real constant. See Dyachenko & Hur (2019), for instance, for details. An integration over one period reveals that

$$\begin{aligned}&(c^2+2b)\mathcal{H}y'-(g+\omega c)y-g(y\mathcal{H}y'+\mathcal{H}(yy'))\\&\quad-\tfrac{1}{2}\omega^2(y^2+\mathcal{H}(y^2y')+y^2\mathcal{H}y'-2y\mathcal{H}(yy'))\\&\quad+g\langle y(1+\mathcal{H}y')\rangle+\omega c\langle y\rangle+\tfrac{1}{2}\omega^2\langle y^2\rangle=0.\end{aligned} \tag{2.29}$$

Indeed, $\langle\mathcal{H}f'\rangle=0$ for any function f and

$$\langle y^2\mathcal{H}y'\rangle=\frac{1}{2\pi}\int_{-\pi}^{\pi}y^2\mathcal{H}y'\,\mathrm{d}u=-\frac{1}{2\pi}\int_{-\pi}^{\pi}y\mathcal{H}(y^2)'\,\mathrm{d}u=-\langle 2y\mathcal{H}(yy')\rangle. \tag{2.30}$$

https://doi.org/10.1017/jfm.2019.634 Published online by Cambridge University Press

We emphasize that (2.29) is made up of polynomials of y, y' and their Hilbert transforms.

But for any ω, c and $b \in \mathbb{R}$, the left side of (2.29) maps a 2π periodic function to a 2π periodic function of mean zero, whereas the left side of (2.25) maps a 2π periodic function to a 2π periodic function, not necessarily of mean zero. In order to reconcile loss of information from (2.25) to (2.29), Constantin *et al.* (2016), Dyachenko & Hur (2019) supplemented (2.29) with

$$\langle (c^2 + 2b - 2gy)((1 + \mathcal{H}y')^2 + (y')^2) \rangle - \langle (c + \omega y(1 + \mathcal{H}y') - \omega \mathcal{H}(yy'))^2 \rangle = 0. \quad (2.31)$$

But the linearization of (2.29)–(2.31) with respect to y and b is not self-adjoint, whence the conjugate gradient or conjugate residual method is inapplicable. Dyachenko & Hur (2019) employed the generalized minimal residual method, instead, and achieved success. But it becomes impractical for large amplitude waves for large values of positive constant vorticity.

Here we make a change of variables

$$y \mapsto y_0 := y + \eta_0 \quad \text{and} \quad c \mapsto c_0 := c - \omega \eta_0, \quad (2.32a,b)$$

for some $\eta_0 \in \mathbb{R}$, so that $b = 0$ but the linear and nonlinear parts of (2.29) remain invariant otherwise. This works, provided that

$$c^2 + 2b - 2gy = c_0^2 - 2gy_0. \quad (2.33)$$

Moreover, we make a change of variables $y \mapsto y + \eta$ for some $\eta \in \mathbb{R}$, so that the constant part of (2.29) vanishes. The result becomes, by abuse of notation,

$$c^2 \mathcal{H}y' - (g + \omega c)y - g(y\mathcal{H}y' + \mathcal{H}(yy')) - \tfrac{1}{2}\omega^2 (y^2 + \mathcal{H}(y^2 y') + y^2 \mathcal{H}y' - 2y\mathcal{H}(yy')) = 0. \quad (2.34)$$

An integration over one period reveals that

$$g\langle y(1 + \mathcal{H}y') \rangle + \omega c \langle y \rangle + \tfrac{1}{2}\omega^2 \langle y^2 \rangle = 0. \quad (2.35)$$

Conversely, a solution of (2.29)–(2.31) and, hence, (2.34) gives rise to a periodic travelling wave of (2.1), (2.3) and (2.8), provided that

$$u \mapsto (u + \mathcal{H}y(u), y(u)), u \in \mathbb{R}, \text{ is injective} \quad (2.36a)$$

and

$$(1 + \mathcal{H}y'(u))^2 + y'(u)^2 \neq 0 \quad \text{for any } u \in \mathbb{R}. \quad (2.36b)$$

See Dyachenko & Hur (2019), for instance, for details. We merely pause to remark that $u + (\mathcal{H} + \mathrm{i})y(u)$ is the boundary value of a conformal map to the fluid region (see (2.10)).

In what follows, we assume that y is even (see Hur 2007, for instance, for arbitrary vorticity).

To recapitulate, the Stokes wave problem in a constant vorticity flow is to seek a 2π periodic and even function y, satisfying (2.36), which solves (2.34) for some $\omega, c \in \mathbb{R}$. To compare, Dyachenko & Hur (2019) solved (2.29)–(2.31) for y and b.

https://doi.org/10.1017/jfm.2019.634 Published online by Cambridge University Press

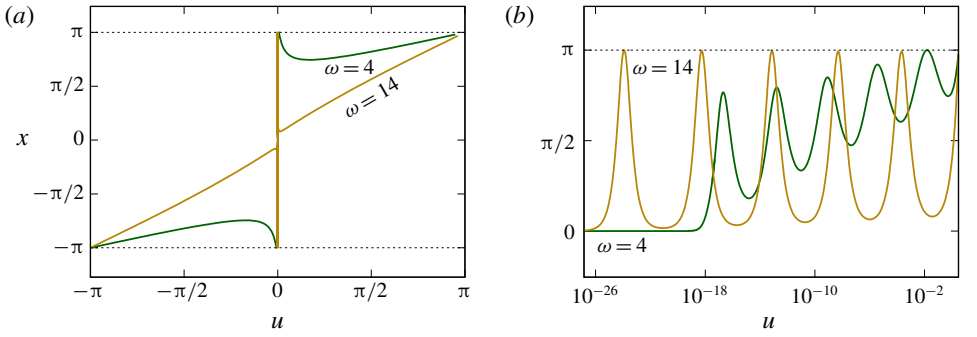


FIGURE 1. (Colour online) The graphs of $x = x(u)$ for two Stokes waves, $\omega = 4.0$ (green) and $\omega = 14.0$ (yellow), where $(x(u), y(u))$, $u \in [-2\pi, 2\pi]$, is a conformal parametrization of a wave profile: on a linear scale (a) and a logarithmic scale (b). See the last column in figure 9 for the profiles.

In the irrotational flow setting, (2.34) becomes the well-known Babenko equation (see Babenko 1987, for instance). One may regard (2.34) as the 'modified Babenko equation', permitting constant vorticity.

We emphasize that the linearization of (2.34)

$$\begin{aligned}\delta y \mapsto\ & c^2\mathcal{H}(\delta y)' - (g + c\omega)\delta y - g(\delta y\mathcal{H}y' + y\mathcal{H}(\delta y)' + \mathcal{H}(y\delta y)')\\ & - \tfrac{1}{2}\omega^2(2y\delta y + \mathcal{H}(y^2\delta y)' - [2y\delta y, y] + [y^2, \delta y]),\end{aligned} \tag{2.37}$$

where $[f_1, f_2] = f_1\mathcal{H}f_2 - f_2\mathcal{H}f_1$, is self-adjoint, whereby we may employ the conjugate gradient method for efficient numerical solution. As a result, we achieve a high numerical precision for large amplitude waves for unprecedentedly large values of constant vorticity.

3. Numerical method

3.1. *Auxiliary conformal coordinates*

Dyachenko *et al.* (2016) and others discussed that in the irrotational setting, a Stokes wave defines the boundary value of a conformal mapping $z = z(w)$ for $w := u + \mathrm{i}v \in \mathbb{C}^-$, and an analytical continuation of z to $\mathbb{C}$ possesses complex singularities in $[\mathrm{i}v_c, +\mathrm{i}\infty)$, where v_c is the closest singularity of z to $\mathbb{C}^-$, and that

$$z(w) - w = \sum_{k \in \leqslant 0, \mathbb{Z}} \widehat{z}(k)\mathrm{e}^{\mathrm{i}kw}, \quad \text{where } |\widehat{z}(k)| \to e^{-v_c|k|} \text{ as } |k| \to \infty. \tag{3.1}$$

Moreover, $v_c \to 0$ as the profile tends to the wave of greatest height, or the extreme wave, presenting challenges for numerical computation. For instance, Dyachenko *et al.* (2016) took up to $2^{27} \approx 1.3 \times 10^8$ uniform grid points in the u variable for $v_c = 5.93824419\cdots \times 10^{-7}$. Lushnikov *et al.* (2017) devised an auxiliary conformal mapping, involving trigonometric functions, to reduce the number of (non-uniform) grid points to $\sqrt{2^{27}} \approx 4.2 \times 10^4$. See also Dyachenko & Hur (2019) for the constant vorticity setting.

The last column of figure 9 shows two Stokes waves with large constant vorticity and large amplitude parametrized conformally by $(x(u), y(u))$ with $u \in [-\pi, \pi]$.

https://doi.org/10.1017/jfm.2019.634 Published online by Cambridge University Press

Figure 1 demonstrates $x = x(u)$ for these waves. The right panel indicates that the closest singularity of the conformal mapping to $\mathbb{C}^-$ is of the order of 10^{-24}, whence the numerical method of Lushnikov *et al.* (2017), Dyachenko & Hur (2019) would require excessively many grid points.

Here we exploit conformal mappings to vertically slit regions in $\mathbb{C}$, involving Jacobi elliptic functions, for further improvements. We refer the interested reader to Hale & Tee (2009), for instance, for details. For $L > 0$, to be determined, suppose that

$$u(q) = -\pi + 2\mathrm{am}\left(K\frac{\pi + q}{\pi}\,\middle|\,\sqrt{1-L^2}\right) \quad \text{for } q \in \mathbb{R}, \tag{3.2}$$

where am denotes the Jacobi amplitude and K is the complete elliptic integral of the first kind with the elliptic modulus $\sqrt{1-L^2}$ (see Abramowitz & Stegun 1964, for instance). Suppose that (3.2) extends to conformally map $\{q \in \mathbb{C} : -d < \mathrm{Im}\, q < 0\}$ of 2π period in the $\mathrm{Re}\, q$ variable, to $\mathbb{C}^-$ of 2π period in the u variable, $w = u + \mathrm{i}v \in \mathbb{C}^-$, where

$$d = \pi K'/K \tag{3.3}$$

and K' is the complete elliptic integral of the first kind with the modulus L.

An explicit calculation reveals that (3.2) maps the Hilbert transform for the strip of depth d in the q variable to the Hilbert transform in the u variable, so that (2.34) remains invariant in the q variable. See also Silantyev (2019) in the irrotational flow setting.

Moreover, (3.2) maps uniform grid points in the q variable over one period, to highly non-uniform in the u variable. We wish to choose a suitable value of L, so that the inverse of (3.2) maps $\mathrm{i}v_c$, the closest singularity to $\mathbb{C}^-$ in the w variable, to $\mathrm{Im}\, q = d$. Since

$$d \approx \frac{\pi^2}{2}\frac{1}{\log(4/L)} \approx \frac{\pi^2}{2}\frac{1}{\log(8/v_c)} \quad \text{as } v_c \to 0, \tag{3.4}$$

it will considerably enlarge the region of analyticity in the q variable when v_c is small. For instance, if v_c is of the order of 10^{-24} in the w variable then the corresponding singularity is approximately 0.086 in the q variable, and in practice, it necessitates no more than 4096 uniform grid points in the q variable to resolve a numerical solution in quadruple precision.

Remark. Numerical evaluation of Jacobi elliptic functions in (3.2) is prone to catastrophic loss of precision in finite digit arithmetic, and it becomes more dramatic as L decreases. Here we employ Landen transformations to evaluate the Jacobi amplitude and the GNU MPFR library in arbitrary precision floating point arithmetic. We then truncate the result to quadruple precision arithmetic. We employ the arithmetic–geometric mean method to compute complete elliptic integrals. We refer the interested reader to Press *et al.* (1992), Bulirsch (1965), for instance, for details.

Remark. We use (3.4) to approximate the optimal value of L, but the exact value of $\mathrm{i}v_c$, the closest singularity to $\mathbb{C}^-$ in the w variable, is typically unknown *a priori*. When L is smaller than optimal then the inverse of (3.2) maps $\mathrm{i}v_c$ to $\pm a + \mathrm{i}d$ for some $a \in \mathbb{R}$, and d depends on L logarithmically. But if L is larger than optimal then (3.2) no longer maps $\mathrm{i}v_c$ to $\mathrm{Im}\, q = d$, and the Fourier spectrum in the q variable widens.

https://doi.org/10.1017/jfm.2019.634 Published online by Cambridge University Press

3.2. *The Newton-conjugate gradient method*

We write (2.34) in the operator form as

$$\mathcal{G}(y, c, \omega) = 0, \tag{3.5}$$

where $y = y(u(q))$ and q is in (3.2), and we solve it iteratively using the Newton method. Let

$$y^{(n+1)} = y^{(n)} + \delta y^{(n)} \quad \text{for } n = 0, 1, 2, \ldots, \tag{3.6}$$

where $y^{(0)}$ is an initial guess, to be supplied, and $\delta y^{(n)}$ solves

$$\delta\mathcal{G}(y^{(n)}, c, \omega)\delta y^{(n)} = -\mathcal{G}(y^{(n)}, c, \omega), \tag{3.7}$$

where $\delta\mathcal{G}(y^{(n)}, c, \omega)$ is the linearization of $\mathcal{G}(y, c, \omega)$ with respect to y and evaluated at $y = y^{(n)}$ (see (2.37)).

We take uniform grid points in the q variable over one period. We approximate $y^{(n)}$ by a discrete Fourier transform and numerically evaluate using a fast Fourier transform. We numerically approximate polynomials of $y^{(n)}$, $(y^{(n)})'$ and their Hilbert transforms likewise and, hence, $\mathcal{G}(y^{(n)}, c, \omega)$ and $\delta\mathcal{G}(y^{(n)}, c, \omega)$.

We numerically solve (3.7) using the conjugate gradient (CG) method (see Yang 2009, 2010, for instance) in the Fourier space for the q variable. Here we choose the linear part of $\mathcal{G}(y^{(n)}, c, \omega)$ as a preconditioner. See Dyachenko *et al.* (2016), for instance, for details. We merely pause to remark that $\delta\mathcal{G}(y^{(n)}, c, \omega)$ may not be positive definite, but the CG method converges nonetheless. To compare, the linearization of (2.29)–(2.31) is not self-adjoint, whence the CG method is inapplicable. Dyachenko & Hur (2019) employed the generalized minimal residual method (see Saad 2003, for instance), instead, and achieved some success. The CG method is more powerful than the generalized minimal residual method for a self-adjoint problem, and we achieve a high numerical precision for large amplitude waves for unprecedentedly large values of constant vorticity.

It turns out that we must supply an initial guess sufficiently close to a true solution of (3.5), so that the Newton-CG method will converge. We begin by taking $\omega = 0$ and a numerical solution of small amplitude (see Dyachenko *et al.* 2016, for instance), and we continue the solution along in ω and c, if necessary, by taking the prior convergent solution as the initial guess and solving (3.5) until we arrive at a solution for the desired ω. See Dyachenko & Hur (2019), for instance, for details. We then fix ω and continue the numerical solution along in c.

But the results in § 4 (see also Dyachenko & Hur 2019) reveal that for ω positive and large, a gap of 'inadmissible' solutions appears in the wave speed versus amplitude plane. Moreover, the gap becomes abnormally large in size as ω increases, so that it is impractical or even numerically prohibited to continue along in c to trace out the gap. For instance, figure 5 indicates that for $\omega = 2.4$ or larger, the wave speed reaches the order of hundreds or larger in the gap. We then take a smaller ω and an admissible numerical solution and we continue along in ω and c, if necessary, until we arrive at an admissible solution for the desired ω. See Dyachenko & Hur (2019), for instance, for details.

The results herein are carried out in quadruple precision floating point arithmetic. We say that the Newton method converges if the residuals $\lesssim N^{1/2}10^{-28}$, where N is the number of uniform grid points in the q variable. We take N sufficiently large, so that the Fourier coefficient $\lesssim N^{-1/2}10^{-26}$ at the wavenumber N, to guarantee that the error in approximating a numerical solution by a discrete Fourier transform is inconsequential. To compare, Dyachenko & Hur (2019) required the residuals less than 10^{-13} and the Fourier coefficients less than 10^{-12}.

https://doi.org/10.1017/jfm.2019.634 Published online by Cambridge University Press

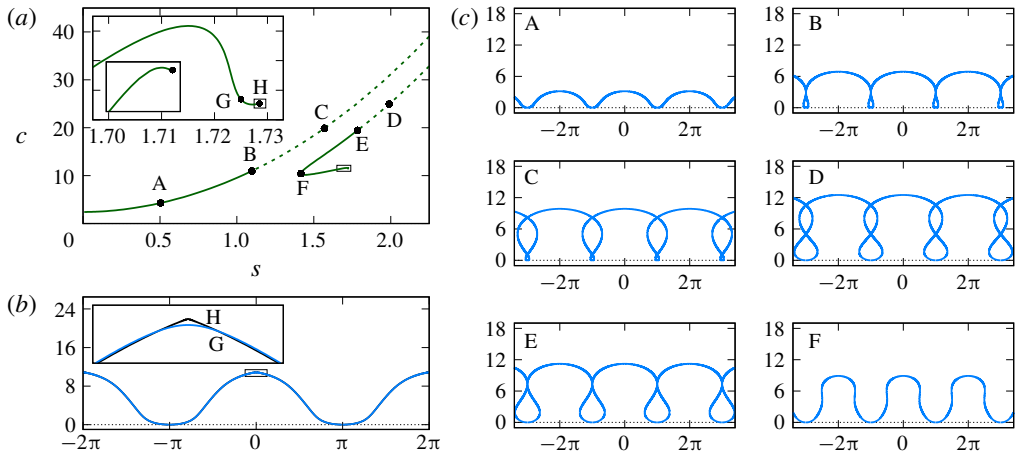


FIGURE 2. (Colour online) Case $\omega = 2$. (*a*) Wave speed versus steepness. Solid curves are for admissible solutions and dashed curves are inadmissible. The insets are close-ups near the endpoint of the continuation of the numerical solution. (*c*) Wave profiles of six solutions, in the (x, y) plane in the range $x \in [-4\pi, 4\pi]$, labelled by A through F in the $c = c(s)$ curve. Troughs are at $y = 0$. (*b*) Profiles of two almost extreme waves, in the (x, y) plane in the range $x \in [-2\pi, 2\pi]$, labelled by G and H in the $c = c(s)$ curve. The inset is a close-up in the vicinity of the crests. We calculate $s = 0.503850870$ (A), 1.09717902 (B), 1.56853350 (C), 1.98985623 (D), 1.78406376 (E), 1.41626450 (F), 1.72499793 (G), 1.72849105 (H).

4. Results

We proceed as in Simmen & Saffman (1985), Teles da Silva & Peregrine (1988) and others, and assume that c is positive but allow ω to be positive or negative. Indeed, if y and c solve (2.34) for some ω then so do y and $-c$ for $-\omega$. We take for simplicity $g = 1$. Recall that the period is 2π. Vanden-Broeck (1996) introduced dimensionless vorticity and gravity parameters, but they depend on c.

In what follows, s denotes the steepness, the crest-to-trough wave height divided by the period, and c measures the wave speed, for which $\langle y(1 + \mathcal{H}y')\rangle = 0$. This is what Simmen & Saffman (1985), Teles da Silva & Peregrine (1988), Dyachenko & Hur (2019) chose, among others.

4.1. *Folds and gaps*

For a large value of positive constant vorticity, Simmen & Saffman (1985) discovered, and Dyachenko & Hur (2019) rediscovered, that the steepness increases, decreases and increases during the continuation of the numerical solution of the Stokes wave problem. Namely, a fold appears in the wave speed versus steepness plane. Moreover, as the value of the vorticity increases, 'inadmissible' solutions make a gap in the wave speed versus steepness plane.

For instance, for $\omega = 2.0$, figure 2(*a*) collects the wave speed versus steepness from the continuation of the numerical solution of (2.34). Figures 2(*b*) and 2(*c*) display, in the (x, y) plane, the wave profiles of eight solutions, labelled by A through H along the $c = c(s)$ curve, in the order in which they appear in the numerical continuation. Here the troughs are at $y = 0$. This is in excellent agreement with Simmen &

https://doi.org/10.1017/jfm.2019.634 Published online by Cambridge University Press

Saffman (1985) figures 10 and 11, qualitatively and quantitatively. A caveat is that the vorticity of Simmen & Saffman (1985) differs in sign. We refer the interested reader to Simmen & Saffman (1985), Dyachenko & Hur (2019), among others, for ω negative, or positive but small.

Figure 2(*a*) reveals a fold in the $c = c(s)$ curve, along which s increases and decreases. For s small, for instance, for wave A, the profile is the graph of a single valued function. But we observe that the profile becomes more rounded as s increases along the fold, so that overhanging waves appear, whose profile is no longer the graph of a single valued function. Moreover, a touching wave follows, whose profile contacts with itself at the trough line, enclosing a bubble of air. For instance, wave B is an almost touching wave.

We report that a numerical solution turns inadmissible past the touching wave because (2.36*a*) no longer holds true. For instance, for wave C, the profile intersects itself and the fluid region overlaps itself. We observe that the wave profile becomes less rounded as s decreases along the fold, so that another touching wave appears. Moreover, a numerical solution turns admissible past the touching wave. For instance, wave D is inadmissible, wave E is an almost touching wave and wave F makes an admissible solution past the touching wave. Together, a gap exists in the $c = c(s)$ curve, which consists of inadmissible numerical solutions and which is bounded by two touching waves. Throughout, we distinguish admissible and inadmissible solutions by solid and dashed curves in the wave speed versus steepness plane. We note that wave E encloses a larger bubble of air than wave B.

We merely pause to remark that the numerical method of Simmen & Saffman (1985) and others diverges in a gap. In stark contrast, the numerical method herein converges throughout. However, we discontinue inadmissible numerical solution when c becomes very large. Instead, we take a smaller ω and an admissible numerical solution and we continue the solution along in ω and c, if necessary. See Dyachenko & Hur (2019), for instance, for details.

The insets of figure 2(*a*) suggest that s increases monotonically past the end of the fold, from $s = 0$ to wave F, while c experiences oscillations, as in the irrotational flow setting (see Dyachenko *et al.* 2016; Lushnikov *et al.* 2017, for instance). Figure 2(*b*) suggests that overhanging waves disappear as s increases past the end of the fold. Moreover, the inset reveals that the crests become sharper, as when $\omega = 0$. We claim that an extreme wave appears ultimately, which is distinguished by peaking at the crest. One may not continue the numerical solution past the extreme wave because (2.36*b*) no longer holds true. For instance, wave H is an almost extreme wave, and we calculate $s = 1.72849105$. This is noticeably higher than the celebrated wave of greatest height, or the extreme wave, in the irrotational setting (see Dyachenko *et al.* 2016, for instance). But the extreme wave here is no longer the wave of greatest height. For instance, for wave E, we calculate $s = 1.78406376$. Simmen & Saffman (1985) estimated the extreme wave steepness ≈ 1.727.

For a larger value of the positive constant vorticity, we take matters further and discover a second fold and a second gap in the wave speed versus steepness plane.

For instance, for $\omega = 2.4$, in figure 3(*a*) is the $c = c(s)$ curve from the continuation of the numerical solution of (2.34), and in figures 3(*b*) and 3(*c*) are the wave profiles of ten solutions at the indicated points along the $c = c(s)$ curve. Figure 3(*a*) reveals a fold from $s = 0$ to wave D, and a gap, bounded by waves B and C, as in figure 2. The profile of wave A is the graph of a single valued function. Wave B is an almost touching wave near the beginning of the gap, and overhanging waves appear somewhere between waves A and B. Wave C is an almost touching wave near the

https://doi.org/10.1017/jfm.2019.634 Published online by Cambridge University Press

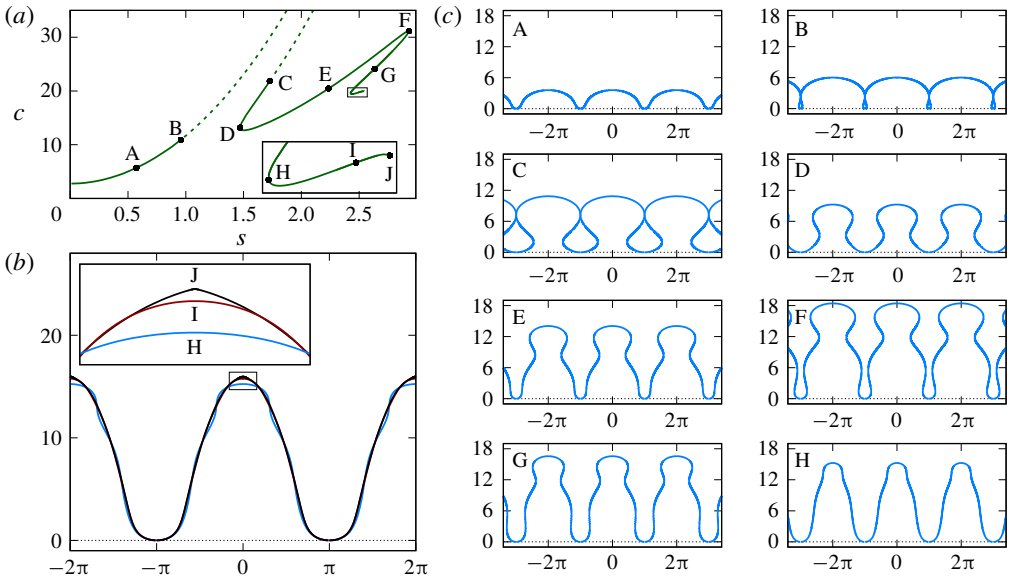


FIGURE 3. (Colour online) Case $\omega = 2.4$. (a) Wave speed versus steepness. Solid and dashed curves are for admissible and inadmissible solutions, respectively. The inset is a close-up near the endpoint of the continuation of the numerical solution. (c) Wave profiles of eight solutions, in the (x, y) plane in the range $x \in [-4\pi, 4\pi]$, labelled by A through H in the $c = c(s)$ curve. Troughs are at $y = 0$. (b) Profiles of three almost extreme waves, in the (x, y) plane in the range $x \in [-2\pi, 2\pi]$, labelled by H through J in the $c = c(s)$ curve. The inset is a close-up in the vicinity of the crests. Calculated are $s = 0.573200642$ (A), 0.957675558 (B), 1.72658434 (C), 1.47087316 (D), 2.23495148 (E), 2.93113607 (F), 2.63473573 (G), 2.42592859 (H), 2.51059898 (I), 2.54343994 (J).

end of the gap. A numerical solution in the gap becomes inadmissible because (2.36a) no longer holds true. Wave D is near the end of the fold.

Moreover, figure 3(a) reveals that s increases from waves D to F, decreases from waves F to H and increases past wave H. Together, another fold, waves D to H, exists in the $c = c(s)$ curve.

The inset of figure 3(a) suggests that s increases monotonically past the end of the second fold, waves D to H, while c experiences oscillations, as in figure 2. Figure 3(b) suggests that overhanging waves disappear as s increases past the end of the second fold. Moreover, the inset reveals that the crests become sharper, like when $\omega = 2.0$. Therefore, we claim that an extreme wave appears ultimately as s increases past the end of the second fold, and one may not continue the numerical solution past the extreme wave, because (2.36b) no longer holds true. For instance, wave J is an almost extreme wave.

For $\omega = 2.5$, figure 4 shows the $c = c(s)$ curve and a selection of wave profiles at the indicated points along the $c = c(s)$ curve. Figure 4(a) reveals the lowest fold, from $s = 0$ to wave D, and a gap, bounded by waves B to C, and the second fold, waves D to F, as in figure 3.

We observe that the wave profile becomes more rounded as s increases along the second fold, so that a touching wave appears, as along the lowest fold. For instance, wave E is an almost touching wave. We observe that a numerical solution turns inadmissible past the touching wave. For instance, for wave F, the profile intersects

https://doi.org/10.1017/jfm.2019.634 Published online by Cambridge University Press

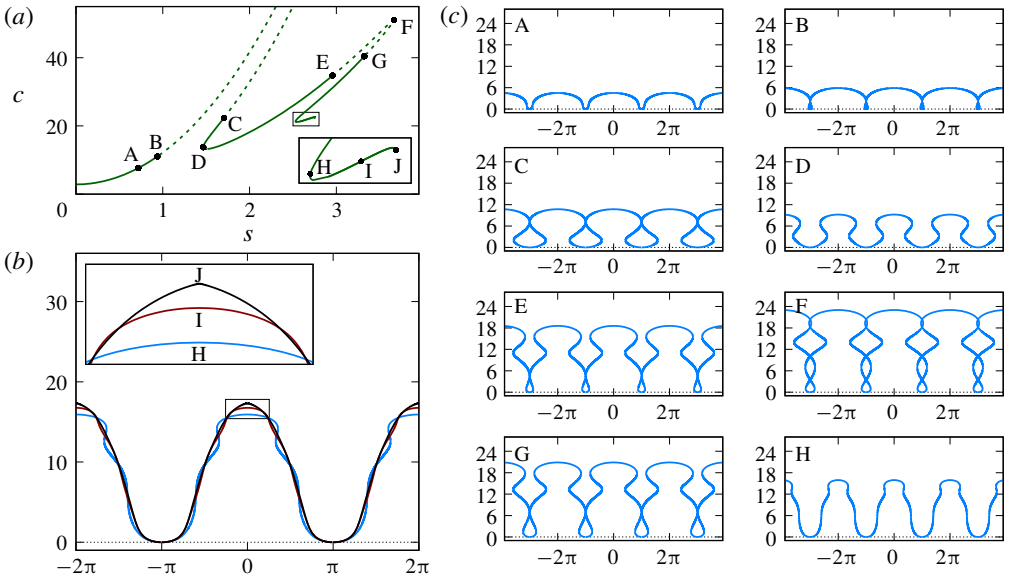


FIGURE 4. (Colour online) Case $\omega = 2.5$. (*a*) Wave speed versus steepness. Solid and dashed curves are for admissible and inadmissible solutions. The inset is a close-up near the endpoint of the continuation of the numerical solution. (*c*) Wave profiles of eight solutions, labelled by A through H in the $c = c(s)$ curve. (*b*) Profiles of three almost extreme waves, labelled by H through J in the $c = c(s)$ curve. The inset is a close-up in the vicinity of the crests; $s = 0.717362459$ (A), 0.936525732 (B), 1.70366636 (C), 1.46562329 (D), 2.95530377 (E), 3.66248662 (F), 3.32175345 (G), 2.53446504 (H), 2.66613185 (I), 2.75929056 (J).

itself and the fluid region overlaps itself. We observe that the wave profile becomes less rounded as s decreases along the second fold, so that another touching wave appears. Moreover, a numerical solution turns admissible past the touching wave, as along the lowest fold. For instance, wave G is an almost touching wave and wave H makes an admissible solution past the touching wave. Together, a second gap exists in the second fold, consisting of inadmissible numerical solutions and bounded by two touching waves.

We merely pause to remark that the numerical method of Simmen & Saffman (1985) and others diverges in a gap. In order to seek admissible numerical solutions past the gap, Simmen & Saffman (1985) took $\omega = 0$ and an almost extreme wave, assuming that (2.36*b*) no longer holds true for the extreme wave, and they continued the numerical solution along in ω and c, if necessary, until they arrived at an almost extreme wave for the desired ω. They continued the numerical solution along in c until they arrived at an almost touching wave, past which their numerical method would diverge. This works, provided that there is one gap, but it is incapable of finding a second gap. To the best of the authors' knowledge, the second gap reported herein is novel. The numerical method of Dyachenko & Hur (2019) converges in a gap, but it takes too much time to accurately resolve solutions along the second fold.

Figure 4(*a*) suggests that s increases monotonically past the second fold, waves D to H, while c experiences oscillations, as in figure 3. Moreover an extreme wave appears ultimately as s increases past the second fold. For instance, wave J is an almost extreme wave.

https://doi.org/10.1017/jfm.2019.634 Published online by Cambridge University Press

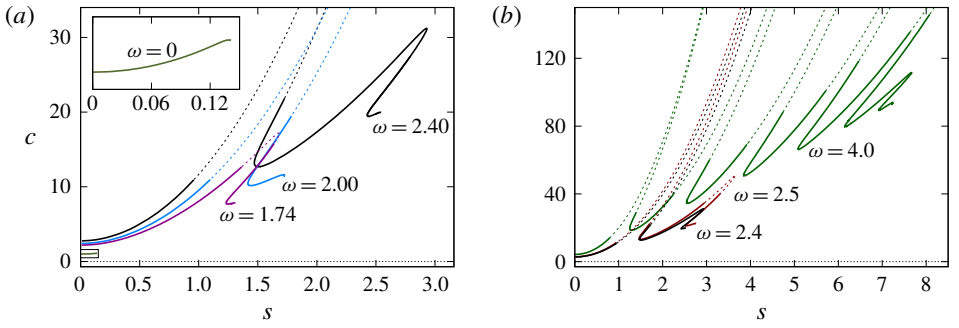


FIGURE 5. (Colour online) Wave speed versus steepness. On (*a*), for $\omega = 0$ (green), 1.74 (magenta), 2.0 (blue), 2.4 (black) and on (*b*), for $\omega = 2.4$ (black), 2.5 (red), 4.0 (green). Solid curves are for admissible solutions and dashed curves for inadmissible ones. The inset is a close-up for $\omega = 0$.

To recapitulate, figure 5 includes the wave speed versus steepness for several values of positive constant vorticity. For zero vorticity, Longuet-Higgins & Fox (1978) and others predicted that the wave speed experiences infinitely many oscillations while the steepness increases monotonically toward the wave of greatest height. Numerical computations (see Dyachenko *et al.* 2016; Lushnikov *et al.* 2017, for instance, and references therein) bear this out. The inset of figure 5(*a*) reproduces it. For negative constant vorticity, the crests become sharper and lower (see Simmen & Saffman 1985; Teles da Silva & Peregrine 1988; Dyachenko & Hur 2019, for instance). For a large value of positive constant vorticity, on the other hand, we find that the lowest oscillation of the wave speed deforms into a fold and, as the value of the vorticity increases, part of the fold transforms into a gap. For instance, for $\omega = 1.74$, figure 5(*a*) displays a fold and a gap. We refer the interested reader to Simmen & Saffman (1985), Dyachenko & Hur (2019), for instance, for details. We observe that the lowest fold and the lowest gap become larger in size as ω increases.

Moreover, for a larger value of the vorticity, for instance, for $\omega = 2.4$, the figure reveals that the second oscillation of the wave speed deforms into another fold. As the value of the vorticity increases, for instance, for $\omega = 2.5$, figure 5(*b*) reveals that part of the second fold transforms into another gap. We observe that the second fold and the second gap become larger in size as ω increases. Furthermore, we find that higher folds and higher gaps develop in like manner. For instance, for $\omega = 4.0$, figure 5(*b*) reveals five folds and five gaps.

We observe that the steepness increases monotonically past all folds, although the wave speed experiences oscillations. Moreover, overhanging waves disappear as s increases past all folds, and the crests become sharper, as in the irrotational setting. Therefore, we claim that an extreme wave appears ultimately, which is distinguished by peaking at the crest. For instance, figure 6 includes almost extreme waves for three values of positive constant vorticity. Moreover, the figure suggests that the extreme wave exhibits a 120° peaking at the crest for any constant vorticity.

4.2. *Touching waves in the infinite vorticity limit*

Interestingly, Dyachenko & Hur (2019) discovered that for a sufficiently large value of positive constant vorticity, touching waves at the boundaries of the lowest gap have capillary effects.

https://doi.org/10.1017/jfm.2019.634 Published online by Cambridge University Press

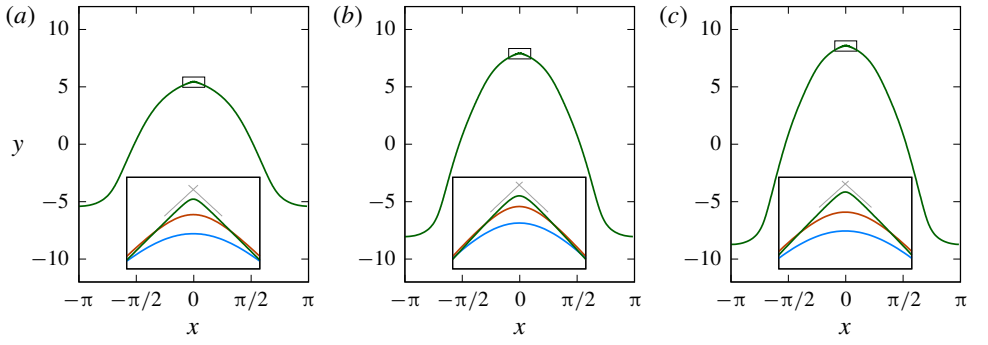


FIGURE 6. (Colour online) Almost extreme waves: $\omega = 2.0$ (a), $\omega = 2.4$ (b) and $\omega = 2.5$ (c), in the (x, y) plane in the range $x \in [-\pi, \pi]$. The mean fluid level is at $y = 0$. The insets are close-ups in the vicinities of the crests. The asymptotics make a 120° angle. We calculate $s = 1.72914844(\omega = 2.0),\ 2.54357018(\omega = 2.4),\ 2.75939536(\omega = 2.5)$.

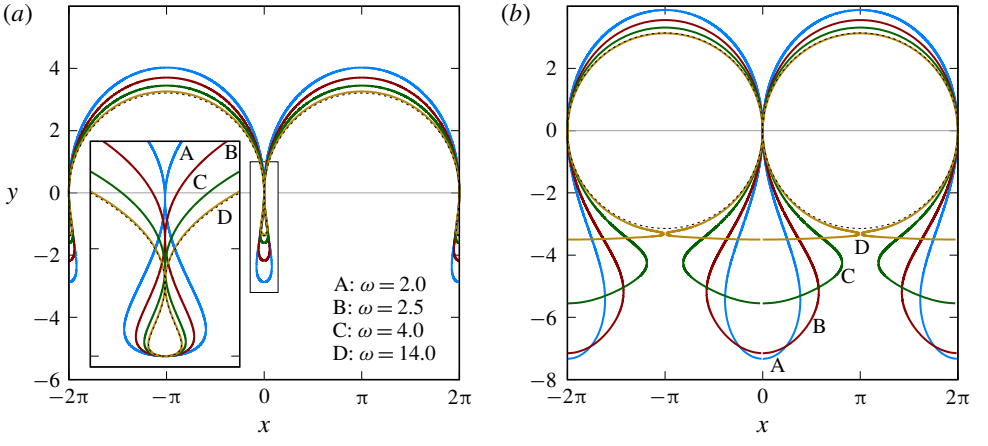


FIGURE 7. (Colour online) (a) Profiles of almost touching waves near the beginnings of the lowest gaps for $\omega = 2.0$ (A, blue), 2.5 (B, red), 4.0 (C, green) and 14.0 (D, yellow), in the (x, y) plane in the range $x \in [-2\pi, 2\pi]$; $s = 1.09717902(\omega = 2.0),\ 0.93652573(\omega = 2.5),\ 0.80492141(\omega = 4.0),\ s = 0.73575899(\omega = 14.0)$. The dashed curve represents the limiting Crapper wave in the infinite vorticity limit. The inset is a close-up in the vicinity of bubbles of air. (b) Almost touching waves near the ends of the gaps. We calculate $s = 1.78406173(\omega = 2.0),\ 1.70366636(\omega = 2.5),\ 1.41081893(\omega = 4.0),\ 1.05512149(\omega = 14.0)$. The dashed curve represents a circle in the infinite vorticity limit. Touching is at $y = 0$.

Figure 7(a) displays the profiles of almost touching waves near the beginnings of the lowest gaps for four values of positive constant vorticity. They resemble the profile in Vanden-Broeck (1996) figure 4(b). We observe that s decreases monotonically toward ≈ 0.73 as $\omega \to \infty$. See Dyachenko & Hur (2019), for instance, for details. In the irrotational setting, Crapper (1957) produced an exact solution of the capillary wave problem (in the absence of gravitational effects). He deduced that the crests become more rounded as the amplitude increases, opposite to gravity waves, and that the wave of greatest height is distinguished by the profile of a touching wave, for which $s \approx 0.730$. Moreover, figure 7(a) reveals that for instance, for $\omega = 14.0$, the profile of an almost touching wave matches remarkably well the limiting Crapper wave. Therefore, we claim that touching waves at the beginnings of the lowest gaps

https://doi.org/10.1017/jfm.2019.634 Published online by Cambridge University Press

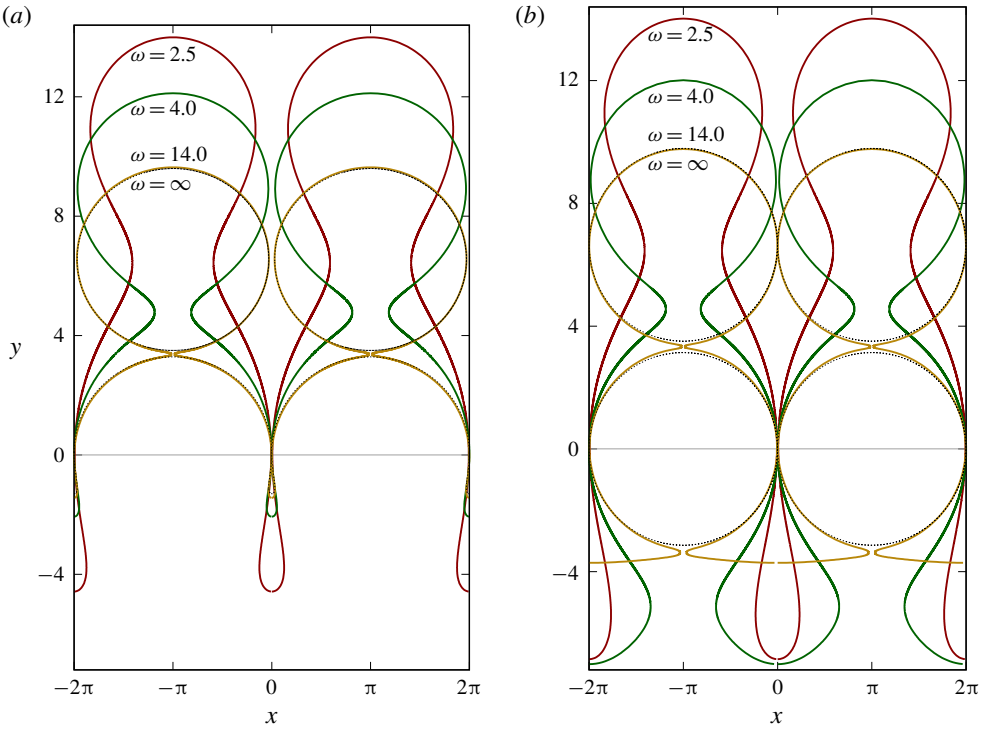


FIGURE 8. (Colour online) (*a*) Profiles of almost touching waves near the beginnings of the second gaps for $\omega = 2.5$ (red), 4.0 (green) and 14.0 (yellow), in the (x, y) plane in the range $[-2\pi, 2\pi]$; $s = 2.95530378(\omega = 2.5)$, $2.25812560(\omega = 4.0)$, $1.76253642(\omega = 14.0)$. The dashed curve represents a circle on top of the limiting Crapper wave in the infinite vorticity limit. (*b*) Almost touching waves near the ends of the gaps; $s = 3.32175345(\omega = 2.5)$, $3.02783846(\omega = 4.0)$, $2.14573393(\omega = 14.0)$. The dashed curve represents a circle on top of itself.

tend to the limiting Crapper wave as the value of positive constant vorticity increases indefinitely. This reveals a striking and surprising link between rotational and capillary effects.

In figure 7(*b*) are the profiles of almost touching waves near the ends of the lowest gaps for four values of positive constant vorticity. We observe that $s \to 1$ as $\omega \to \infty$. Teles da Silva & Peregrine (1988) numerically computed 'pure rotational waves' in a constant vorticity flow, in the absence of gravitational effects, and argued that a limiting wave is distinguished by a circular configuration of fluid in rigid body rotation. Moreover, figure 7(*b*) reveals that, for instance, for $\omega = 14.0$, the profile of an almost touching wave is nearly circular. Therefore, we claim that touching waves at the ends of the lowest gaps tend to the 'circular vortex wave' as $\omega \to \infty$ or, equivalently, $g \to 0$ while $\omega > 0$ is held fixed.

Moreover, in figure 8(*a*) are the profiles of almost touching waves near the beginnings of the second gaps, and in figure 8(*b*), profiles of almost touching waves near the ends of the gaps, for three values of positive constant vorticity. The profile on figure 8(*a*) for $\omega = 14.0$ resembles that in Vanden-Broeck (1996), figure 5(*c*), and the profile on figure 8(*b*) resembles that in Vanden-Broeck (1996), figure 6. The figures suggest that touching waves at the beginnings of the second gaps tend

https://doi.org/10.1017/jfm.2019.634 Published online by Cambridge University Press

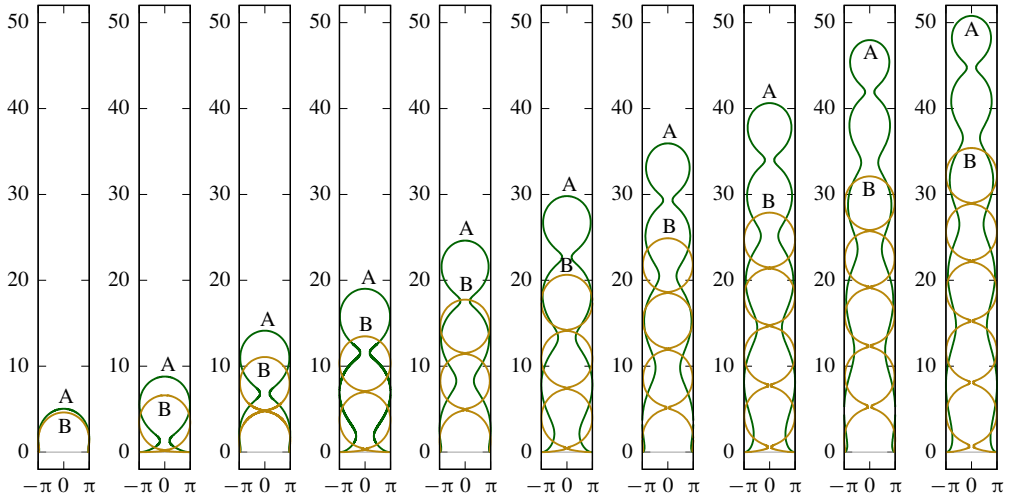


FIGURE 9. (Colour online) The profiles of almost touching waves at the beginnings and ends of the five gaps for $\omega = 4.0$ (A, green) and $\omega = 14$ (B, yellow), in the (x, y) plane in the range $x \in [-\pi, \pi]$; $s = 0.80374141,\ 1.40058987,\ 2.25089824,\ 3.02783845,\ 3.91928481,\ 4.74312194,\ 5.72000991,\ 6.46604675,\ 7.63328861,\ 8.08151762$ $(\omega = 4.0)$; $s = 0.735758992,\ 1.05379349,\ 1.76253641,\ 2.14573392,\ 2.82520536,\ 3.28534733,\ 3.96265847,\ 4.43686502,\ 5.10919552,\ 5.63398162$ $(\omega = 14.0)$.

to circular vortex wave on top of a limiting Crapper wave as the value of positive constant vorticity increases indefinitely, while the circular vortex wave on top of itself at the end of the gaps in the infinite vorticity limit, or the zero gravity limit.

We claim that touching waves at the boundaries of higher gaps accommodate more circular bubbles of fluid in like manner. For instance, figure 9 displays almost touching waves near the beginnings and ends from the lowest to fifth gaps for two large values of positive constant vorticity, and suggests that touching waves at the beginnings of the nth gaps tend to $n - 1$ circular vortex waves on top of the limiting Crapper wave, while n circular vortex waves at the ends of the gaps as $\omega \to \infty$.

5. Discussion

Here we modify Babenko's nonlinear pseudodifferential equation for Stokes waves (see Babenko 1987, for instance), to allow constant vorticity. It is useful for high precision numerical computation, and we are able to continue the numerical solution, from zero amplitude up to an extreme wave, for a very large value of positive constant vorticity, which seems daunting for the formulation in Dyachenko & Hur (2019) and others.

This leads to some important discoveries, stimulating further analytical and numerical investigations. As the value of positive constant vorticity increases, more folds and gaps appear in the wave speed versus amplitude plane. But past all folds, the amplitude increases monotonically toward an extreme wave, which is distinguished by a 120° peaking at the crest, regardless of the value of vorticity. The extreme wave is not in general a wave of greatest height. Moreover, touching waves at the beginnings of the lowest gaps tend to the limiting Crapper wave (see Crapper 1957, for instance) in the infinite vorticity limit or, equivalently, zero gravity limit, suggesting a striking and surprising link between rotational and capillary effects.

https://doi.org/10.1017/jfm.2019.634 Published online by Cambridge University Press

Some of 'exotic' waves, such as those in the last column of figure 9, or perhaps all, are likely to be unstable. But it is a matter of analysis to understand their instability, which may be relevant to some physical processes. We intend to numerically investigate stability in the future. High precision numerical solutions serve an important preliminary result. Moreover, we modify the equations in Zakharov *et al.* (2002), for instance, for unsteady waves, to allow constant vorticity, which will be useful for the purpose.

Acknowledgements

V.M.H. is supported by the National Science Foundation under the Faculty Early Career Development (CAREER) Award DMS-1352597. S.D. is supported by the National Science Foundation under DMS-1716822. The authors thank the anonymous referees for helpful comments and suggestions.

REFERENCES

ABRAMOWITZ, M. & STEGUN, I. A. 1964 *Handbook of Mathematical Functions with Formulas, Graphs, and Mathematical Tables (National Bureau of Standards Applied Mathematics Series)*, vol. 55. For sale by the Superintendent of Documents, U.S. Government Printing Office, Washington, D.C.

BABENKO, K. I. 1987 Some remarks on the theory of surface waves of finite amplitude. *Soviet Math. Doklady* **35** (6), 599–603.

BULIRSCH, R. 1965 Numerical calculation of elliptic integrals and elliptic functions. *Numer. Math.* **7**, 78–90.

CONSTANTIN, A., STRAUSS, W. & VĂRVĂRUCĂ, E. 2016 Global bifurcation of steady gravity water waves with critical layers. *Acta Math.* **217** (2), 195–262.

CRAPPER, G. D. 1957 An exact solution for progressive capillary waves of arbitrary amplitude. *J. Fluid Mech.* **2**, 532–540.

DOSAEV, A. S., TROITSKAYA, Y. I. & SHISHINA, M. I. 2017 Simulation of surface gravity waves in the Dyachenko variables on the free boundary of flow with constant vorticity. *Fluid Dyn.* **52** (1), 58–70.

DYACHENKO, A. I., KUZNETSOV, E. A., SPECTOR, M. D. & ZAKHAROV, V. E. 1996 Analytical description of the free surface dynamics of an ideal fluid (canonical formalism and conformal mapping). *Phys. Lett.* A **221** (1), 73–79.

DYACHENKO, S. A. & HUR, V. M. 2019 Stokes waves with constant vorticity: I. Numerical computation. *Stud. Appl. Maths* **142**, 162–189.

DYACHENKO, S. A., LUSHNIKOV, P. M. & KOROTKEVICH, A. O. 2016 Branch cuts of Stokes wave on deep water. Part I: Numerical solution and Padé approximation. *Stud. Appl. Maths* **137** (4), 419–472.

EWING, J. A. 1990 Wind, wave and current data for the design of ships and offshore structures. *Mar. Struct.* **3** (6), 421–459.

HALE, N. & TEE, T. W. 2009 Conformal maps to multiply slit domains and applications. *SIAM J. Sci. Comput.* **31** (4), 3195–3215.

HUR, V. M. 2007 Symmetry of steady periodic water waves with vorticity. *Phil. Trans. R. Soc. Lond.* A **365** (1858), 2203–2214.

LONGUET-HIGGINS, M. S. & FOX, M. J. H. 1978 Theory of the almost-highest wave. II. Matching and analytic extension. *J. Fluid Mech.* **85** (4), 769–786.

LUSHNIKOV, P. M. 2016 Structure and location of branch point singularities for Stokes waves on deep water. *J. Fluid Mech.* **800**, 557–594.

LUSHNIKOV, P. M., DYACHENKO, S. A. & SILANTYEV, D. A. 2017 New conformal mapping for adaptive resolving of the complex singularities of Stokes wave. *Proc. R. Soc. Lond.* A **473** (2202), 20170198.

https://doi.org/10.1017/jfm.2019.634 Published online by Cambridge University Press

PEREGRINE, D. H. 1976 Interaction of water waves and currents. In *Advances in Applied Mechanics*, vol. 16, pp. 9–117. Elsevier.

PRESS, W. H., TEUKOLSKY, S. A., VETTERLING, W. T. & FLANNERY, B. P. 1992 *Numerical Recipes in C*, 2nd edn. Cambridge University Press.

SAAD, Y. 2003 *Iterative Methods for Sparse Linear Systems*, 2nd edn. Society for Industrial and Applied Mathematics.

SILANTYEV, D. A. 2019 A new conformal map for computing Stokes wave.

TELES DA SILVA, A. F. & PEREGRINE, D. H. 1988 Steep, steady surface waves on water of finite depth with constant vorticity. *J. Fluid Mech.* **195**, 281–302.

SIMMEN, J. A. & SAFFMAN, P. G. 1985 Steady deep-water waves on a linear shear current. *Stud. Appl. Maths* **73** (1), 35–57.

STOKES, G. G. 1847 On the theory of oscillatory waves. *Trans. Camb. Phil. Soc.* **8**, 441–473.

STOKES, G. G. 1880 *Mathematical and Physical Papers*, vol. 1. Cambridge University Press.

SWAN, C., CUMMINS, I. P. & JAMES, R. L. 2001 An experimental study of two-dimensional surface water waves propagating on depth-varying currents. Part 1. Regular waves. *J. Fluid Mech.* **428**, 273–304.

VANDEN-BROECK, J.-M. 1996 Periodic waves with constant vorticity in water of infinite depth. *IMA J. Appl. Maths* **56** (2), 207–217.

YANG, J. 2009 Newton-conjugate-gradient methods for solitary wave computations. *J. Comput. Phys.* **228** (18), 7007–7024.

YANG, J. 2010 *Nonlinear Waves in Integrable and Nonintegrable Systems, Mathematical Modeling and Computation*, vol. 16. Society for Industrial and Applied Mathematics (SIAM).

ZAKHAROV, V. E., DYACHENKO, A. I. & VASILYEV, O. A. 2002 New method for numerical simulation of a nonstationary potential flow of incompressible fluid with a free surface. *Eur. J. Mech. (*B*/Fluids)* **21** (3), 283–291.

ZYGMUND, A. 1959 *Trigonometric Series*, 2nd edn. vol. I, II. Cambridge University Press.

https://doi.org/10.1017/jfm.2019.634 Published online by Cambridge University Press